Cell Reports

Hippo-released WWC1 facilitates AMPA receptor regulatory complexes for hippocampal learning

Graphical abstract

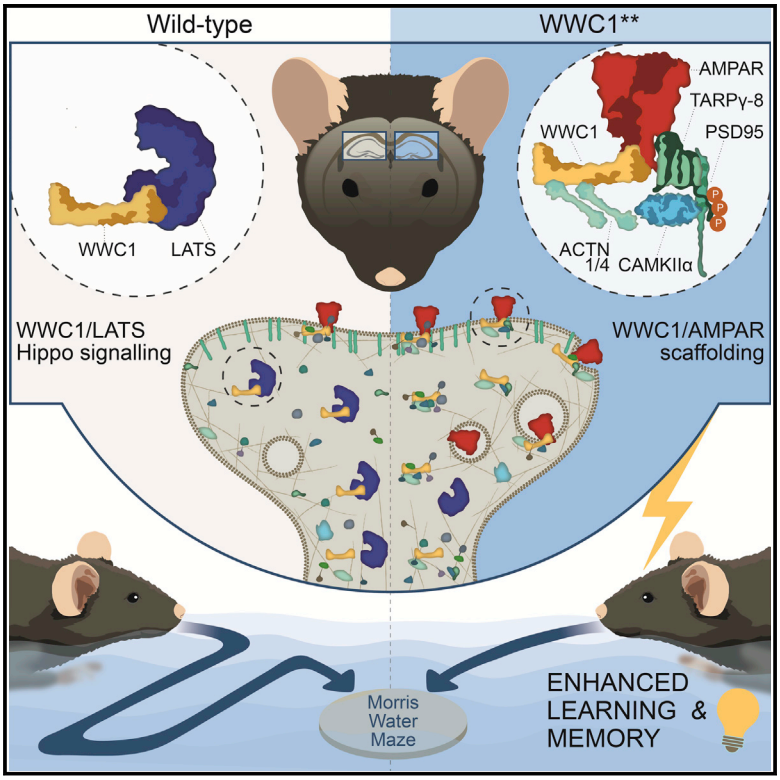

Highlights

- Multilevel proteomics show WWC1 as a major postsynaptic hub for AMPA receptor complexes
- WWC1/LATS dissociation enhances AMPA receptor scaffolds on the postsynaptic site
- WWC1/LATS dissociation primes long-term memory in mice

Authors

Jens Stepan, Daniel E. Heinz, Frederik Dethloff, ..., Joachim Kremerskothen, Carsten T. Wotjak, Nils C. Gassen

Correspondence

stepan@psych.mpg.de (J.S.), wotjak@psych.mpg.de (C.T.W.), nils.gassen@ukbonn.de (N.C.G.)

In brief

Stepan et al. report that the memory-enhancing effects of the Hippo pathway member WWC1 rely on its binding to LATS. Upon WWC1/LATS dissociation, WWC1 becomes an important component of postsynaptic AMPA receptor heterocomplexes and improves long-term memory in mice.

Stepan et al., 2022, Cell Reports *41*, 111766
December 6, 2022
https://doi.org/10.1016/j.celrep.2022.111766

Cell Reports

CellPress
OPEN ACCESS

Report

Hippo-released WWC1 facilitates AMPA receptor regulatory complexes for hippocampal learning

Jens Stepan,[1,2,3,*] Daniel E. Heinz,[2,4,5] Frederik Dethloff,[1,6] Thomas Bajaj,[2] Andreas Zellner,[2,7] Kathrin Hafner,[1] Svenja Wiechmann,[7,8,9] Sarah Mackert,[2] Yara Mecdad,[2] Michael Rabenstein,[11] Tim Ebert,[2,4] Silvia Martinelli,[1] Alexander S. Häusl,[10,12] Maximilian L. Pöhlmann,[10,12] Anke Hermann,[13] Xiao Ma,[14] Hermann Pavenstädt,[13] Mathias V. Schmidt,[10,12] Alexandra Philipsen,[15] Chris W. Turck,[1] Jan M. Deussing,[16] Bernhard Kuster,[7,8,9,17] Michael C. Wehr,[14] Valentin Stein,[11] Joachim Kremerskothen,[13] Carsten T. Wotjak,[4,18,*] and Nils C. Gassen[1,2,19,*]

[1]Department of Translational Research in Psychiatry, Max Planck Institute of Psychiatry, 80804 Munich, Germany
[2]Research Group Neurohomeostasis, Department of Psychiatry and Psychotherapy, University Hospital Bonn, 53127 Bonn, Germany
[3]Department of Obstetrics and Gynecology, Paracelsus Medical University, 5020 Salzburg, Austria
[4]Research Group Neuronal Plasticity, Max Planck Institute of Psychiatry, 80804 Munich, Germany
[5]Max Planck School of Cognition, 04103 Leipzig, Germany
[6]Metabolomics Core Facility, Max Planck Institute for Biology of Ageing, 50931 Cologne, Germany
[7]Chair of Proteomics and Bioanalytics, Technical University of Munich, 85354 Freising, Germany
[8]German Cancer Consortium (DKTK), 80336 Munich, Germany
[9]German Cancer Center (DKFZ), 69120 Heidelberg, Germany
[10]Department Stress Neurobiology and Neurogenetics, Max Planck Institute of Psychiatry, 80804 Munich, Germany
[11]Institute of Physiology II, University Hospital Bonn, 53115 Bonn, Germany
[12]Research Group Neurobiology of Stress Resilience, Max Planck Institute of Psychiatry, 80804 Munich, Germany
[13]Department of Medicine D, Division of General Internal Medicine, Nephrology, and Rheumatology, University Hospital Münster, 48149 Münster, Germany
[14]Research Group Signal Transduction, Department of Psychiatry and Psychotherapy, University Hospital, LMU Munich, 80336 Munich, Germany
[15]Clinic for Psychiatry and Psychotherapy, University Hospital Bonn, 53127 Bonn, Germany
[16]Research Group Molecular Neurogenetics, Max Planck Institute of Psychiatry, 80804 Munich, Germany
[17]Bavarian Center for Biomolecular Mass Spectrometry, Technical University of Munich, 85354 Freising, Germany
[18]Central Nervous System Diseases Research, Boehringer-Ingelheim Pharma GmbH & Co KG, 88400 Biberach, Germany
[19]Lead contact
*Correspondence: stepan@psych.mpg.de (J.S.), wotjak@psych.mpg.de (C.T.W.), nils.gassen@ukbonn.de (N.C.G.)
https://doi.org/10.1016/j.celrep.2022.111766

SUMMARY

Learning and memory rely on changes in postsynaptic glutamergic α-amino-3-hydroxy-5-methyl-4-isoxazolepropionic acid (AMPA)-type receptor (AMPAR) number, spatial organization, and function. The Hippo pathway component WW and C2 domain-containing protein 1 (WWC1) regulates AMPAR surface expression and impacts on memory performance. However, synaptic binding partners of WWC1 and its hierarchical position in AMPAR complexes are largely unclear. Using cell-surface proteomics in hippocampal tissue of *Wwc1*-deficient mice and by generating a hippocampus-specific interactome, we show that WWC1 is a major regulatory platform in AMPAR signaling networks. Under basal conditions, the Hippo pathway members WWC1 and large tumor-suppressor kinase (LATS) are associated, which might prevent WWC1 effects on synaptic proteins. Reduction of WWC1/LATS binding through a point mutation at WWC1 elevates the abundance of WWC1 in AMPAR complexes and improves hippocampal-dependent learning and memory. Thus, uncoupling of WWC1 from the Hippo pathway to AMPAR-regulatory complexes provides an innovative strategy to enhance synaptic transmission.

INTRODUCTION

Despite multiple dimensions of cognition, learning and memory performance shape our personality and individuality in a unique manner (Dere et al., 2010; Millan et al., 2012). Brain diseases such as Alzheimer's disease (AD), as well as age-associated cognitive decline, are characterized by temporary or permanent loss of memory (Masters et al., 2015; Gan et al., 2018). Consequently, intensive research efforts are being made to identify mechanisms that normalize the underlying signaling cascades and brain circuits (Husain and Mehta, 2011; Lynch et al., 2014; Brogi et al., 2019).

Glutamatergic α-amino-3-hydroxy-5-methyl-4-isoxazolepropionic acid-type receptors (AMPARs) mediate the majority of fast, excitatory neurotransmission in the brain (Granger et al., 2013; Diering and Huganir, 2018). Their number, spatial organization, and function at the postsynapse are most strongly and specifically implicated in synaptic plasticity, learning, and memory (Granger et al., 2013; Penn et al., 2017; Diering and Huganir, 2018; Groc and Choquet, 2020). Thus, innovative strategies to control AMPAR number and/or signaling properties to enhance cognitive performance would be highly desirable (Lynch et al., 2014; Brogi et al., 2019). The activity-dependent adaptation of functionally responsive AMPARs can take place by lateral diffusion between extrasynaptic and synaptic compartments and/or by alignment in front of presynaptic release sites (Borgdorff and Choquet, 2002; Penn et al., 2017; Groc and Choquet, 2020). Furthermore, their biophysical properties and turnover are defined by (1) their assembly to homo- or heterotetramers from four highly homologous pore-forming GLUA (1–4) subunits; (2) their direct and indirect association with various subunit-specific interacting proteins (e.g., transmembrane AMPAR-regulatory proteins [TARPs], cornichon proteins [CNIHs], membrane-associated guanylate kinase homologs [MAGUKs]); and (3) subunit-specific posttranslational modifications (PTMs; Schwenk et al., 2012; Granger et al., 2013; Brechet et al., 2017; Diering and Huganir, 2018; Bissen et al., 2019).

Even though the vast repertoire of AMPAR phenotypes entails ample opportunities for drug design, their direct manipulation by agonists or positive allosteric modulators has largely failed in patients (Lynch et al., 2014; Bernard et al., 2019; Brogi et al., 2019). This might be ascribed, at least in part, to an aging- or dementia-related reduced availability of AMPARs on postsynaptic sites (Moore et al., 1993; Yang et al., 2015; Gan et al., 2018; Martín-Belmonte et al., 2020). Here, we modify the WW and C2 domain-containing protein 1 (WWC1; Yu et al., 2015; Papassotiropoulos et al., 2006) to link AMPARs to protein-hetero complexes, which might promote their cell surface expression.

WWC1 emerged as a promising target for the following reasons: first, the association between human memory performance and an intronic SNP (rs17070145) within the *WWC1* gene (Papassotiropoulos et al., 2006; Bates et al., 2009; Milnik et al., 2012), and second, the link between neuronal WWC1 and AMPAR regulation in rodents (Kremerskothen et al., 2005; Makuch et al., 2011; Vogt-Eisele et al., 2014; Heitz et al., 2016; Tracy et al., 2016; Ji et al., 2019; Fukuda et al., 2019). WWC1, also known as kidney and brain (KIBRA), is one of several upstream regulatory proteins of the Hippo signaling pathway (Genevet et al., 2010; Wang et al., 2014; Yu et al., 2015). The core kinases in the Hippo pathway are mammalian sterile 20-like protein kinases 1 and 2 (MST1/2; also known as STK3/4) and large tumor-suppressor kinases 1 and 2 (LATS1/2). The resulting Hippo signaling cascade is a major focus of research on tissue proliferation, organ growth, and cancer (Dong et al., 2007; Lei et al., 2008; Yu et al., 2015). Nevertheless, the memory-enhancing effects of WWC1 have sparked extensive research on its neuronal function (Büther et al., 2004; Johannsen et al., 2008; Makuch et al., 2011; Vogt-Eisele et al., 2014; Blanque et al., 2015; Heitz et al., 2016; Tracy et al., 2016; Ji et al., 2019).

WWC1 is highly expressed on postsynaptic sites in brain regions relevant for learning and memory, such as the hippocampus and cerebellum (Kremerskothen et al., 2003; Johannsen et al., 2008; Makuch et al., 2011; Heitz et al., 2016; Tracy et al., 2016). Moreover, it contains an N-terminal WW domain tandem (Kremerskothen et al., 2005; Lin et al., 2019; Ji et al., 2019); an internal phospholipid-interacting C2 domain (Duning et al., 2013); a binding site for atypical protein kinase C (aPKC) (Vogt-Eisele et al., 2014); and a C-terminal-binding PDZ motif (Vogt-Eisele et al., 2014) (Figure S2A). Candidate-based studies have identified a few WWC1 binding partners implicated in AMPAR physiology including protein interacting with C kinase 1 (PICK1), Dendrin, PKMζ, and cytoskeletal proteins (Kremerskothen et al., 2003, 2005; Büther et al., 2004; Duning et al., 2008; Makuch et al., 2011; Vogt-Eisele et al., 2014; Blanque et al., 2015; Heitz et al., 2016; Tracy et al., 2016; Ji et al., 2019; Fukuda et al., 2019). Altogether, this suggests that WWC1 scaffolds direct communication between AMPARs and AMPAR-regulating proteins (Makuch et al., 2011; Wang et al., 2014; Lin et al., 2019). However, as few WWC1 interactors have been documented so far (Kremerskothen et al., 2005; Makuch et al., 2011; Vogt-Eisele et al., 2014; Heitz et al., 2016; Tracy et al., 2016; Ji et al., 2019; Fukuda et al., 2019), the complete network of WWC1 synaptic binding partners that define its hierarchical position in postsynaptic AMPAR macromolecules remains obscure.

Overexpressed WWC1 promotes AMPAR expression (Heitz et al., 2016; Tracy et al., 2016), begging the question of how its availability is regulated at the crossroads between Hippo signaling and synaptic processes. While Xiao et al. (2011) showed that the interaction of WWC1 and LATS regulates Hippo pathway activity, its effects on neuronal networks has not been explicitly investigated. We hypothesized that pro-cognitive effects of WWC1 rely on its ability to scaffold plasticity-related postsynaptic proteins, the extent of which, in turn, depends on synaptic WWC1 availability that could be regulated within the Hippo pathway. We explored this hypothesis using an unbiased proteomic approach and by providing the "master switch" directing WWC1's fate toward either the Hippo or synaptic signaling networks. Our multilevel proteomic data and the molecular mechanism of WWC1 regulation were then evaluated for behavioral outcomes by manipulating WWC1 availability in mice.

The results demonstrate how dissociation of WWC1 from LATS and, thus, decoupling from the Hippo pathway shapes higher-order brain function by redirecting information flow in postsynaptic signaling networks. WWC1 facilitates the physical assembly of AMPAR hetero-protein complexes and thereby promotes learning and memory in mice. Our results lead to a deep mechanistic understanding of WWC1 regulation to promote synaptic function.

RESULTS

Identification of the WWC1-dependent hippocampal membranome

WWC1 is critical for AMPAR trafficking (Makuch et al., 2011; Heitz et al., 2016; Tracy et al., 2016; Ji et al., 2019), but very little is known about its role in synaptic signaling networks. Thus, we applied a two-pronged strategy to identify and validate WWC1-dependent candidates in neurons, followed by exploration of

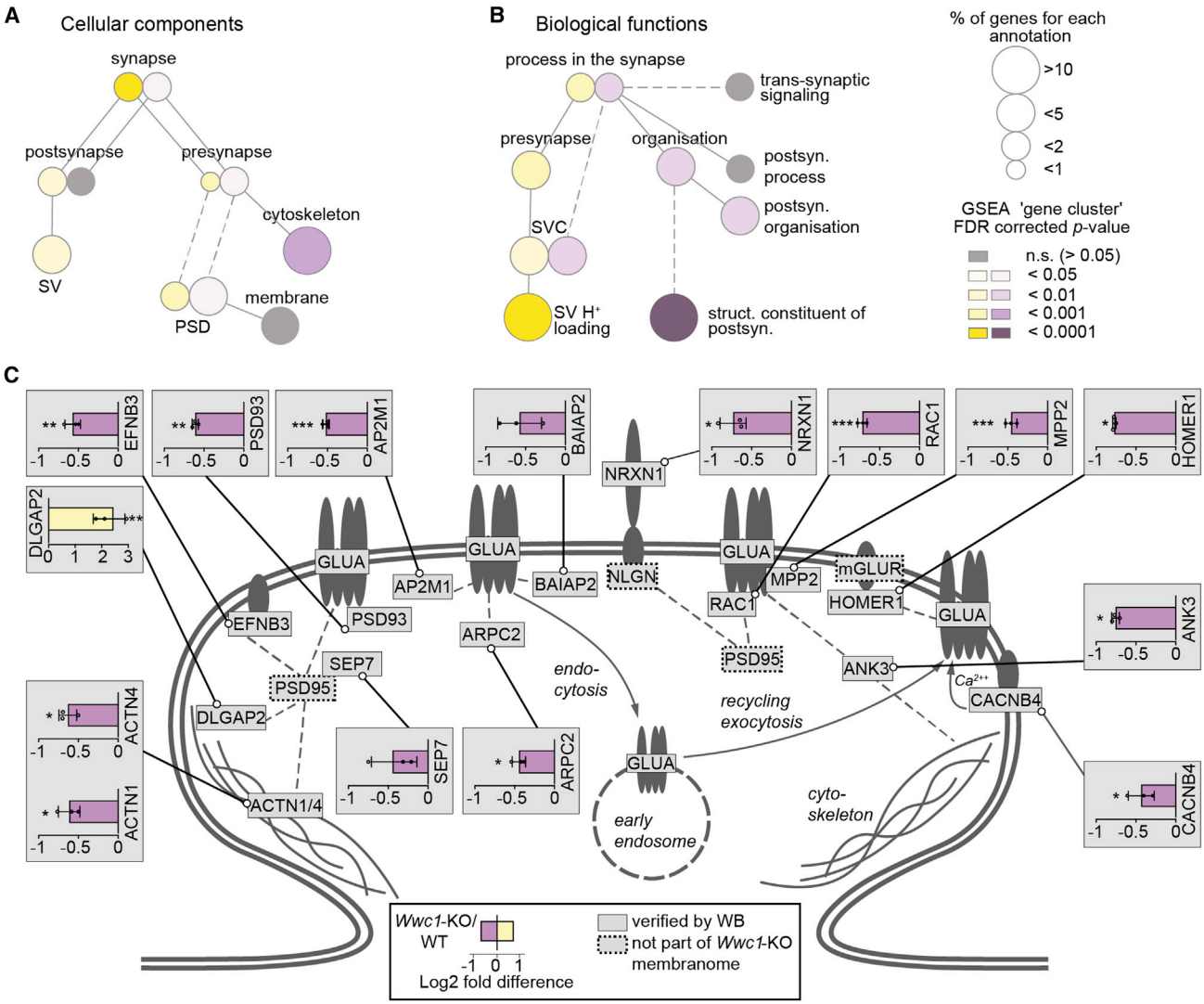

Figure 1. WWC1-dependent hippocampal membrane proteomics

(A and B) Gene Ontology analysis of changed proteins by SynGO. Cellular component (A) and biological function (B) enrichment analysis of membrane proteins (for statistical information see also Table S1; SV, synaptic vesicle; PSD, postsynaptic density; SVC, synaptic vesicle cycle).

(C) Scheme illustrating the validation of AMPAR-related membrane proteins identified. Proteins were enriched as described in Figure S1A and quantified by western blot (WB). Scale indicates log2 fold difference compared with WT (*$p < 0.05$, **$p < 0.01$, ***$p < 0.001$, two-tailed unpaired t tests, n = 3 mice per group; see also Table S1).

Data are mean ± SEM.

their AMPAR-regulating properties (Figures 1A–1C; Figures S1 and S2). We started with an unbiased proteomic approach (Loh et al., 2016) to identify the landscape of WWC1-dependent membranomic changes in the dorsal hippocampus of *Wwc1* knockout (*Wwc1*-KO) mice (Vogt-Eisele et al., 2014) and wild-type (WT) littermate controls. We labeled primary amine groups of membrane proteins with cell-impermeable biotins, followed by streptavidin affinity purification (Figure S2A; Gabriel et al., 2014). Subsequently, we performed mass spectrometry (MS)-based proteomics with label-free quantification (LFQ; Loh et al., 2016) to enable proteomic mapping of the neuronal surface. We identified 2,927 proteins associated with neuronal membranes (Figures S2B–S2D; Table S1), highlighting 213 protein expression changes—57 enriched and 156 reduced—in the hippocampus of *Wwc1*-KO mice (Figures S2B–S2D; Table S1). To estimate the efficiency of biotin labeling of surface proteins, we lysed biotinylated brain slices and used a dot-blot technique in combination with an HRP-conjugated streptavidine. We could show a strong labeling efficiency of up to 2,500% (Figure S2E).

Using an evidence-based and systematic gene-annotation analysis of synaptic proteins (SynGO; Koopmans et al., 2019), we found that more than 10% (23/213) of WWC1-dependent neuronal proteins were associated with synaptic components and functions (Figures 1A and 1B). In-depth analysis revealed

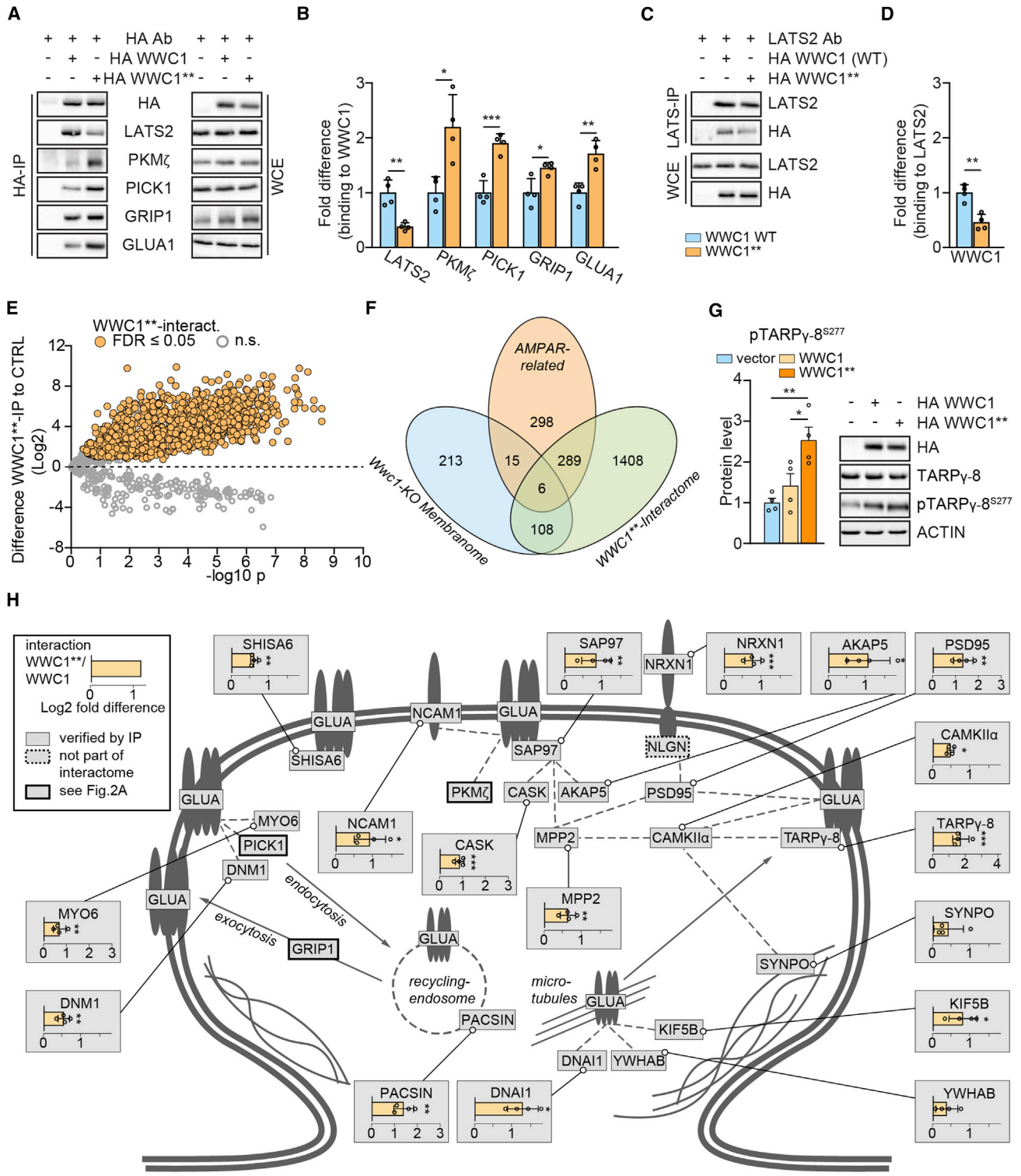

Figure 2. Mutant WWC1 segregates from LATS to modulate AMPAR scaffolds

(A) Co-immunoprecipitation (IP) of overexpressed HA WWC1 (WT) or HA WWC1** in primary hippocampal neurons. Protein extracts were used for IP of HA-tagged proteins using either control immunoglobulin G (IgG) or anti-HA antibody. Detection of immunoprecipitated HA-tagged WWC1 proteins and endogenous LATS2, PKMζ, PICK1, GRIP1, and GLUA1, respectively (WCE, whole-cell extract).

(B) Quantification of data from (A) (**p = 0.0022, *p = 0.0111, ***p = 0.0006, *p = 0.0174, **p = 0.0034, two-tailed unpaired t tests, n = 4 mice).

(C) Representative immunoblots for HA and LATS2.

(legend continued on next page)

that the majority of proteins with reduced expression were linked to postsynaptic components (Figure 1A; Table S1) and functions (Figure 1B; Table S1). In contrast, the majority of enriched proteins were associated with presynaptic components (Figure 1A; Table S1) and functions (Figure 1B; Table S1). This suggests that the pattern of WWC1-dependent protein changes causes a shift in pre- and postsynaptic balance, which may reflect compensatory processes (Futai et al., 2007).

It is known that changes in postsynaptic AMPAR number, organization, and function are critical for hippocampus-dependent learning and memory (Bissen et al., 2019; Groc and Choquet, 2020). Thus, we asked whether any altered membrane proteins in *Wwc1*-KO mice are associated with AMPAR regulation. Importantly, these mice had normal levels of AMPARs in hippocampal protein extracts (Figure S2F). Indeed, 15 of the 213 WWC1-dependent membrane-expressed proteins were associated with AMPARs and were further validated by western blot (WB; Figure 1C; Figure S2G; Table S1). Within this group, only DLGAP2 was enhanced, while the remaining proteins were reduced in membrane precipitates of *Wwc1*-KO mice (Figure 1C; Figure S2G; Table S1). We noted decreased levels of AMPAR regulators, including cytoskeleton-associated proteins (Neurexin1, Homer1, α-actinin), postsynaptic scaffolders (PSD93), and the inner core AMPAR auxiliary protein MPP2 (Figure 1C; Figure S2G; Table S1). Accordingly, these data indicate a hotspot of WWC1-associated proteins implicated in various forms of AMPAR regulation in the postsynaptic compartment.

Mutant WWC1 segregates from LATS to scaffold AMPAR heterocomplexes

Previous research has shown that overexpression of WWC1 in HEK293 cells shapes Hippo pathway activity through the binding and subsequent stabilization of LATS1/2 (Xiao et al., 2011). In addition, elevated WWC1 protein promotes basal and activity-dependent GLUA1 trafficking and facilitates synaptic plasticity in the rodent brain (Heitz et al., 2016; Tracy et al., 2016). This duality of protein function prompted us to hypothesize that WWC1's interaction with LATS1/2 plays a decisive role in setting its primary fate either within the Hippo pathway or in synaptic regulatory networks. To shift WWC1 from its role in Hippo signaling toward regulation of synaptic processes, we antagonized the WWC1-LATS2 interaction by overexpressing WWC1, which harbors a double point mutation (P37/84A) in the two WW domains known to be crucial for binding LATS2 (Figure S3A). Adeno-associated virus (AAV)-mediated overexpression of the hemagglutinin (HA)-tagged WWC1** mutant in primary hippocampal neurons followed by co-immunoprecipitation (coIP) revealed strongly reduced binding between HA-WWC1** and LATS2, and vice versa, compared with overexpressed HA-WWC1 WT (Figures 2A–2D). At the same time, it resulted in an enhanced interaction with AMPAR-binding partners PKMζ (Vogt-Eisele et al., 2014), GRIP1 (Dong et al., 1997), PICK1 (Makuch et al., 2011), and GLUA1 (Figures 2A and 2B). Furthermore, chemical induction of long-term potentiation (cLTP) in brain slices reduced WWC1-LATS binding (Figure S3B), suggesting that the dissociation of WWC1 and LATS2 occurs in hippocampal neurons following stimuli associated with synaptic plasticity in mammals (Kopec et al., 2006). Various intracellular constituents are thought to regulate AMPARs either directly or as part of AMPAR hetero-protein complexes (Schwenk et al., 2012; Brechet et al., 2017; Bissen et al., 2019). To complement the membranome data, we next determined the LATS2-segregated WWC1 (WWC1**) interactome in the hippocampus (Maccarrone et al., 2017). By combining HA-affinity purification and label-free proteomics, we identified 1,733 proteins and highlighted 1,408 proteins as significant interactors of WWC1**, including AMPAR subunits 1–4 (Figures 2E and 2F; Table S2). A gene annotation (Gene Ontology [GO]) analysis (Panther database; Thomas et al., 2003) of these 1,408 interactor proteins revealed various enriched cellular components and biological processes (Table S2), consistent with the proposed function of WWC1 as a synaptic scaffolder (Makuch et al., 2011; Wang et al., 2014; Ji et al., 2019; Fukuda et al., 2019). Subsequent SynGO analysis (Koopmans et al., 2019) highlighted enrichment of WWC1** interactors in all of the five main synaptic localizations: presynapse, postsynapse, synaptic membrane, synaptic cleft, and extrasynaptic space (Figure S3C; Table S2). Likewise, functional enrichment revealed involvement of WWC1** in all five annotated biological categories: pre- and postsynaptic processes, synaptic organization, synaptic signaling, axonal and dendritic transport, and metabolism (Figure S3D; Table S2). These data suggest that the majority of WWC1** interactors are associated with neuronal function. Comparison of both proteomic datasets (membranome versus interactome) revealed a substantial overlap of 108 proteins (Figure 2F), highlighting that these proteins are not simply WWC1 interactors but that their translocation to the synaptic membrane is WWC1 dependent. Moreover, literature mining of interactome data revealed 289 neuronal proteins associated with AMPARs (Figure 2F; Figure S3E; Table S2). Next, we validated various proteins including core constituents of AMPAR complexes (e.g., TARPγ-8, MPP2, SHISA6; Schwenk et al., 2012), as well as direct and indirect AMPAR interactors,

(D) Quantification of data from (C) (**p = 0.0020, two-tailed unpaired t test, n = 4 mice).

(E) The WWC1**-dependent interactome identified by liquid chromatography-tandem mass spectrometry (LC-MS/MS) in hippocampal tissue. Significant protein hits are shown in orange (volcano: false discovery rate [FDR] ≤ 0.05, s0 = 0.1, n = 4 mice per group; for further statistical information, see also Table S2).

(F) Venn diagram of the *Wwc1*-KO membranome compared with the WWC1** interactome in hippocampal tissue plus relation to AMPAR function.

(G) Quantification of WBs of pTARPγ-8^{S277} over TARPγ-8 in WWC1** versus WWC1 (WT, i.e., vector-transfected) primary hippocampal neurons ($F_{2, 9}$ = 9.227, **p = 0.0066, one-way ANOVA, *p < 0.05, **p < 0.01, Tukey's post-hoc test, n = 4 for each group). coIP of overexpressed HA-WWC1 (WT) versus HA-WWC1** in primary hippocampal neurons. Protein extracts were used for IP of HA-tagged proteins using either control IgG or anti-HA antibody. Detection of immunoprecipitated HA-tagged WWC1 proteins and endogenous TARPγ-8 and TARPγ-8^{S277}.

(H) Schematic illustrating the validation of AMPAR interactors. coIP was performed as described in (A) using lysates from WWC1** neurons or WWC1 (WT) neurons (or vector-transfected neurons) quantified by WB. Scale indicates fold difference compared with WWC1 (WT) neurons (*p < 0.05, **p < 0.01, ***p < 0.001, two-tailed unpaired t tests, n = 4 mice per group; for further statistical information, see also Table S2).

Data are mean ± SEM.

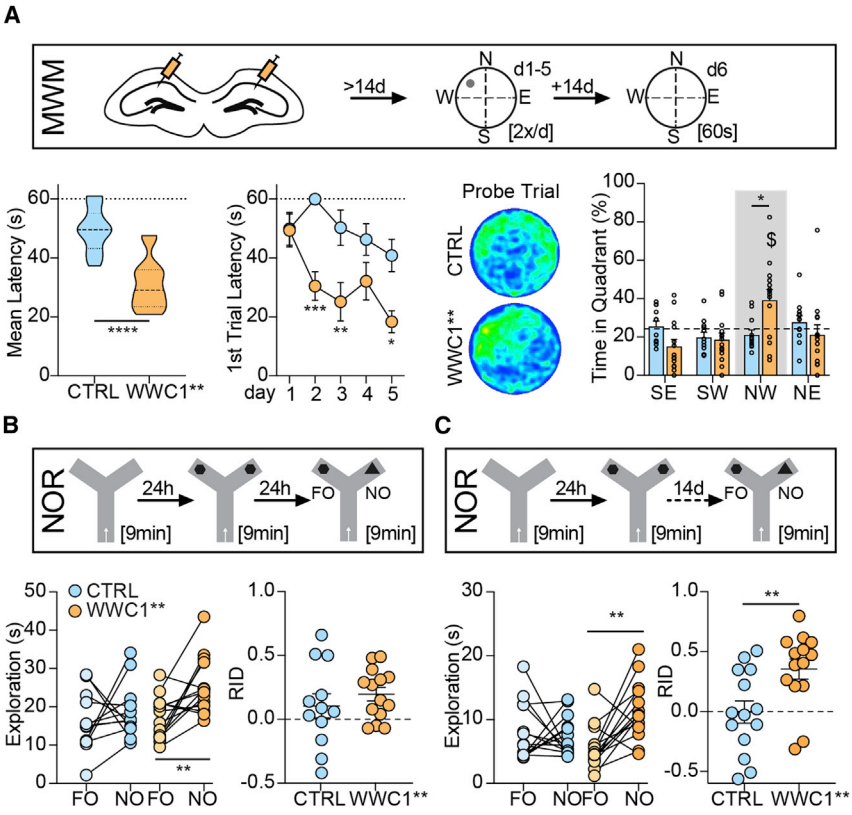

Figure 3. Improved learning and memory in WWC1 mice**

(A) Scheme illustrating the Morris water maze (MWM) with 2 training trials per day. Mean first trial escape latency over the entire training period for WWC1**-overexpressing (WWC1**, n = 14) and control (CTRL; n = 12) mice (****p < 0.0001, two-tailed unpaired t test). Escape latencies during the first trial per day reflecting the consolidation of long-term memory for WWC1** and CTRL mice (virus: $F_{1,24}$ = 33.76, p < 0.0001, two-way repeated measures (RM)-ANOVA; *p < 0.05, **p < 0.01, ***p < 0.001, Bonferroni's post-hoc test). Heatmap representation of the retention times across the experimental groups during the probe trial on day 6 and average time spent in each quadrant (quadrant × virus interaction: $F_{3, 72}$ = 4.161, **p = 0.0089, two-way RM-ANOVA; $p < 0.05 versus other quadrants, *p < 0.05 versus CTRL, Bonferroni's post-hoc test).

(B) Schemes illustrating the novel object recognition (NOR) test performed 14 days after transfection. Exploration time of an NO compared with a familiar object (FO) for WWC1** (n = 14) and CTRL (n = 12) mice 24 h after sampling (*p = 0.4597, **p = 0.004, two-tailed paired t tests). Ratio of investigation duration (RID) for WWC1** and CTRL (p = 0.3923, two-tailed unpaired t test).

(C) Exploration time of an NO compared with an FO for new cohorts of control (CTRL, n = 14) and WWC1** mice (n = 14) 14 days after learning (p = 0.7416, p = 0.0027, two-tailed paired t tests). RID for CTRL and WWC1** mice (p = 0.0081, two-tailed unpaired t test).

Data are mean ± SEM.

such as CAMKIIα or postsynaptic density (PSD) proteins (Figures 2G and 2H; Figure S4; Table S2; Diering and Huganir, 2018; Bissen et al., 2019). Given that TARPγ-8 is predominantly expressed in the hippocampus (Kato et al., 2016) and is a major CAMKIIα substrate critically important for memory processes (Rouach et al., 2005), we selected TARPγ-8 and CAMKIIα for further investigations. Thereby, we found that CAMKIIα-dependent TARPγ-8 phosphorylation is strongly enhanced in WWC1**-expressing primary hippocampal neurons when compared with the corresponding controls (Figure 2G). In order to probe that WWC1 is an important AMPAR regulator, we used a *Wwc1* knockdown or control AAV in mouse hippocampus. In tissue extracts from these mice, we determined TARPγ-8 interaction partners using IP and proteomics (Figure S5A). We identified a large number of AMPAR-relevant proteins whose TARPγ-8 binding behavior is altered by *Wwc1* knockdown (Figure S5B; Table S3). Altogether, these data demonstrate that, when dissociated from LATS, WWC1 becomes an important regulatory nexus for postsynaptic processes that hold the potential for controlling different levels of AMPAR physiology. This includes AMPAR membrane insertion; stabilization; reinsertion after internalization (GRIP1; Dong et al., 1997; Setou et al., 2002); AMPAR internalization and intracellular anchorage (PICK1; Xia et al., 1999; Makuch et al., 2011); AMPAR transport along microtubules (KIF1a, KIF5; Setou et al., 2002; Shin et al., 2003); AMPAR trafficking to and at the (extra) synaptic membrane (PSD93, PSD95, SAP102, TARPγ-8, CAMKIIα; Schnell et al., 2002; Rouach et al., 2005; Elias et al., 2006; Park et al., 2016); and postsynaptic anchoring of AMPARs (Neurexin-1, α-actinin; Mondin et al., 2011; Matt et al., 2018).

Synaptic WWC1 primes hippocampal learning

We next examined whether synaptic WWC1 improves hippocampal learning. Mice overexpressing WWC1** in the CA1 region of the dorsal hippocampus were able to form an improved long-term memory for the platform position in the Morris water maze (MWM) after training with an inefficient learning protocol (Chowdhury and Caroni, 2018) of only two training trials per day (Figure 3A). These memory-enhancing effects became evident from the mean first trial escape latencies over the entire training period, the day-to-day learning progress, and the resulting selective searching for the platform position in the probe trial (Figure 3A). In addition, WWC1**-overexpressing mice, but not controls, were also able to form a 24 h long-term memory of objects in the novel object recognition (NOR) test (Figure 3B), which may last for at least 14 days after learning (Figure 3C).

DISCUSSION

We demonstrate that decoupling of WWC1 from Hippo signaling lays the foundation for tethering postsynaptic AMPAR-containing

hetero-protein complexes to promote the formation of long-term memory. We characterize WWC1 as a major synaptic scaffold protein, whereby our multilevel proteomic approach did not merely recapitulate known neuronal WWC1 binding partners implicated in AMPAR homeostasis but also revealed hitherto unprecedented coverage and depth of WWC1-dependent membrane protein expression and interactors.

One central and widely accepted hypothesis assumes that synaptic plasticity, which underlies hippocampal learning and memory, depends on AMPAR number and spatial organization on postsynaptic sites (Penn et al., 2017; Diering and Huganir, 2018; Groc and Choquet, 2020). This necessitates a diverse pattern of protein interactions, which coordinately guide AMPAR trafficking (Schwenk et al., 2012; Brechet et al., 2017; Diering and Huganir, 2018; Bissen et al., 2019). The spatial and temporal organization of such highly structured molecular signaling networks is accomplished through scaffolding proteins (Elias et al., 2006; MacGillavry et al., 2013). Although recent research strongly suggests that WWC1 is an important scaffold of AMPAR-related postsynaptic proteins (Makuch et al., 2011; Vogt-Eisele et al., 2014; Heitz et al., 2016; Tracy et al., 2016, Ji et al., 2019), its hierarchical position in regulatory AMPAR hetero-protein complexes has not been investigated so far. Here, a spatially restricted enzymatic tagging approach enabled us to separate hippocampal transmembrane proteins from intracellular proteins and thus selectively label, identify, and quantify the *Wwc1*-dependent neuronal membranome (Loh et al., 2016). This strategy, along with the analysis of the WWC1** interactome (Gabriel et al., 2014), demonstrates that WWC1 participates in assembling key molecular components of AMPAR-trafficking networks. In addition to hundreds of previously unknown proteins controlling various aspects of neuronal homeostasis, function, and plasticity, we show that WWC1 interacts with 298 AMPAR-related synaptic proteins including major proteins such as PSD93, PSD95, TARPγ-8, CAMKIIα, and CACNB4 (Schwenk et al., 2012; Brechet et al., 2017; Bissen et al., 2019). These data may provide a mechanistic explanation for the impact of WWC1 on multiple layers of AMPAR physiology (Makuch et al., 2011; Heitz et al., 2016; Tracy et al., 2016; Ji et al., 2019). Notably, we identified WWC1 as a potential scaffolder for two critical steps of AMPAR regulation: first, WWC1 likely modulates the CAMKIIα-dependent phosphorylation of TARPγ-8 at serine 277 (S277; Park et al., 2016), and second, it may also participate in subsequent AMPAR movements and stabilization through scaffolding their interaction with MAGUKs via the PDZ domain of TARPγ-8 (Nicoll et al., 2006).

An essential feature of WWC1 is bidirectional regulation of memory-related processes (Vogt-Eisele et al., 2014; Heitz et al., 2016; Tracy et al., 2016; Ji et al., 2019). Elevated WWC1 levels primarily promote AMPAR surface insertion, synaptic plasticity, learning, and memory, while reduced WWC1 levels favor AMPAR internalization and compromise synaptic plasticity and memory performance (Vogt-Eisele et al., 2014; Heitz et al., 2016; Tracy et al., 2016; Ji et al., 2019). Interestingly, Tracy et al. (2016) found that neuronal levels of WWC1 are downregulated in patients suffering from severe AD. Further, our list of WWC1-dependent, AMPAR-regulating proteins includes additional candidates such as PSD95 (Feyder et al., 2010) or VPS35 (Temkin et al., 2017), which are associated with neuropsychiatric disease. Nevertheless, bidirectional effects of WWC1 on memory processes raise the question of how its neuronal availability is governed and highlight the possibility that targeting WWC1 could be clinically relevant. The strong and specific interaction between WWC1-WW tandem domains and LATS PPxY motifs that had been implicated in Hippo pathway regulation (Xiao et al., 2011; Lin et al., 2019) can be modulated through mutation in the N-terminal WW-domain (Xiao et al., 2011). Here, we show that WWC1/LATS dissociation through the WW-domain mutation induces WWC1 decoupling from proliferation-related Hippo pathway (Yu et al., 2015) and thereby promotes gain of synaptic function. Setting WWC1 regulation apart from the Hippo cascade is fundamentally different from standard approaches such as overexpression systems or genetic knockdown (Makuch et al., 2011; Heitz et al., 2016). These techniques may dramatically disrupt the protein homeostasis of synapses and may not match with the physiological mechanisms underlying WWC1 regulation and availability.

WWC1/LATS dissociation within the dorsal hippocampus enabled the animals to form a long-term memory about the hidden platform upon training with a limited number of daily trials, which was insufficient in control animals (Chowdhury and Caroni, 2018). Moreover, it "converted" short-term into long-term recognition memory, which lasted for the remarkable period of at least 2 weeks.

Together, our data provide strong support for the hypothesis that higher WWC1 accessibility through WWC1/LATS dissociation modulates AMPAR macromolecular complexes, which, in turn, have the potential to counteract disease-related disruption of AMPAR homeostasis and memory processes. The essential role of AMPARs in learning and memory has sparked a debate about the most appropriate pharmacological strategy to improve their function and/or synaptic abundance. Since direct allosteric modulators have largely failed in clinical trials (Lynch et al., 2014; Bernard et al., 2019; Brogi et al., 2019), we propose indirect, WWC1-mediated targeting of AMPAR dynamics as a potential strategy for the development of next-generation cognitive enhancers.

Limitations of the study

A minor limitation of this study is that the method used to determine proteins on the cell membrane does not exclusively allow a distinction between pure membrane proteins and proteins that are bridged by them. On the other hand, the method presented here provides a deeper insight into the membrane-proximal changes caused by *Wwc1* KO (Table S1). This explains that although we demonstrate high biotin-labeling efficiency (Figure S2E), intracellular proteins were likely co-purified with biotinylated transmembrane proteins (Weekes et al., 2010). While our study shows that dissociation from LATS allows WWC1 to regulate AMPAR trafficking, synaptic plasticity, and learning, the mechanism(s) promoting WWC1/LATS dissociation remain(s) to be identified. Therefore, we will assess if the switch from Hippo signaling to AMPAR regulation involves PTMs like protein phosphorylation. Lastly, we demonstrated that the transient expression of WWC1** in the hippocampus enhance AMPAR trafficking and learning. However, we cannot entirely

rule out that expression of WWC1 (WT) causes comparable behavioral effects to WWC1**.

STAR★METHODS

Detailed methods are provided in the online version of this paper and include the following:

- KEY RESOURCES TABLE
- RESOURCE AVAILABILITY
  - Lead contact
  - Materials availability
  - Data and code availability
- EXPERIMENTAL MODEL AND SUBJECT DETAILS
  - Mouse strains
  - Primary cell cultures
- METHOD DETAILS
  - Chemicals
  - Chemical long-term potentiation (cLTP)
  - Morris water maze (MWM)
  - Novel object recognition (NOR)
  - Stereotactic virus injections
  - Membrane protein biotinylation
  - Biotinylation efficiency using dot blot
  - Immunoblot analysis
  - Transfections
  - Co-immunoprecipitation (Co-IP)
  - Label-free quantitative proteomic analysis of membrane proteins and WWC1 interaction partners
  - Panther classification system
  - SynGO
  - Automated literature search
- QUANTIFICATION AND STATISTICAL ANALYSIS

SUPPLEMENTAL INFORMATION

Supplemental information can be found online at https://doi.org/10.1016/j.celrep.2022.111766.

ACKNOWLEDGMENTS

We thank R. Huganir for expression constructs PICK1-GFP and KIBRA-FLAG; S. Tomita for phospho-TARPγ-8 antibody; J. du Hoffmann for editing the manuscript; and B. Steigenberger, N. Krombholz, and N. Nagaraj from the Max Planck Institute of Biochemistry, Core Facility Mass Spectrometry, and S. Bauer and S. Unkmeir for excellent technical support. We thank M. Oliviero for support illustrating the graphical abstract. This work was funded by an NARSAD Young Investigator Award by the Brain and Behaviour Research Foundation, honored by the P&S Fund (to N.C.G., grant ID 25348). D.E.H. was supported by BMBF and Max Planck Society.

AUTHOR CONTRIBUTIONS

Conceptualization, J.S., C.T.W., and N.C.G.; methodology, J.S., C.T.W., and N.C.G.; software, S. Martinelli; formal analysis, F.D., Z.A., S.W., Y.M., C.T.W., and B.K.; investigation, J.S., D.E.H., T.B., K.H., S. Mackert, M.R., T.E., A.S.H., M.L.P., A.H., X.M., and P.A.; resources, H.P., M.V.S., J.M.D., B.K., M.C.W., V.S., J.K., and C.T.W.; data curation, F.D., A.Z., and Y.M.; writing – original draft, J.S. and N.C.G.; writing – review & editing, all authors; visualization, S.J., D.E.H., F.D., T.B., Y.M., C.T.W., and N.C.G.; supervision, J.S., C.T.W., and N.C.G.; project administration, J.S., C.T.W., and N.C.G.; funding acquisition, C.T.W. and N.C.G.

DECLARATION OF INTERESTS

The authors declare no competing interests.

Received: April 8, 2022
Revised: August 23, 2022
Accepted: November 10, 2022
Published: December 6, 2022

REFERENCES

Bates, T.C., Price, J.F., Harris, S.E., Marioni, R.E., Fowkes, F.G., Stewart, M.C., Murray, G.D., Whalley, L.J., Starr, J.M., and Deary, I.J. (2009). Association of KIBRA and memory. Neurosci. Lett. *458*, 140–143.

Bernard, K., Gouttefangeas, S., Bretin, S., Galtier, S., Robert, P., Holthoff-Detto, V., Cummings, J., and Pueyo, M. (2019). A 24-week double-blind placebo-controlled study of the efficacy and safety of the AMPA modulator S47445 in patients with mild to moderate Alzheimer's disease and depressive symptoms. Alzheimers Dement *5*, 231–240.

Bischofberger, J., Engel, D., Li, L., Geiger, J.R.P., and Jonas, P. (2006). Patch-clamp recording from mossy fiber terminals in hippocampal slices. Nat. Protoc. *1*, 2075–2081.

Bissen, D., Foss, F., and Acker-Palmer, A. (2019). AMPA receptors and their minions: auxiliary proteins in AMPA receptor trafficking. Cell. Mol. Life Sci. *76*, 2133–2169.

Blanque, A., Repetto, D., Rohlmann, A., Brockhaus, J., Duning, K., Pavenstädt, H., Wolff, I., and Missler, M. (2015). Deletion of KIBRA, protein expressed in kidney and brain, increases filopodial-like long dendritic spines in neocortical and hippocampal neurons in vivo and in vitro. Front. Neuroanat. *9*, 13.

Borgdorff, A.J., and Choquet, D. (2002). Regulation of AMPA receptor lateral movements. Nature *417*, 649–653.

Brechet, A., Buchert, R., Schwenk, J., Boudkkazi, S., Zolles, G., Siquier-Pernet, K., Schaber, I., Bildl, W., Saadi, A., Bole-Feysot, C., et al. (2017). AMPA-receptor specific biogenesis complexes control synaptic transmission and intellectual ability. Nat. Commun. *8*, 15910.

Brogi, S., Campiani, G., Brindisi, M., and Butini, S. (2019). Allosteric modulation of ionotropic glutamate receptors: an outlook on new therapeutic approaches to treat central nervous system disorders. ACS Med. Chem. Lett. *10*, 228–236.

Büther, K., Plaas, C., Barnekow, A., and Kremerskothen, J. (2004). KIBRA is a novel substrate for protein kinase Czeta. Biochem. Biophys. Res. Commun. *317*, 703–707.

Chowdhury, A., and Caroni, P. (2019). Time units for learning involving maintenance of system-wide cFos expression in neuronal assemblies. Nat. Commun. *10*, 3083.

Cox, J., and Mann, M. (2008). MaxQuant enables high peptide identification rates, individualized p.p.b.-range mass accuracies and proteome-wide protein quantification. Nat. Biotechnol. *26*, 1367–1372.

Dere, E., Pause, B.M., and Pietrowsky, R. (2010). Emotion and episodic memory in neuropsychiatric disorders. Behav. Brain Res. *215*, 162–171.

Diering, G.H., and Huganir, R.L. (2018). The AMPA receptor code of synaptic plasticity. Neuron *100*, 314–329.

Dong, H., O'Brien, R.J., Fung, E.T., Lanahan, A.A., Worley, P.F., and Huganir, R.L. (1997). GRIP: a synaptic PDZ domain-containing protein that interacts with AMPA receptors. Nature *386*, 279–284.

Dong, J., Feldmann, G., Huang, J., Wu, S., Zhang, N., Comerford, S.A., Gayyed, M.F., Anders, R.A., Maitra, A., and Pan, D. (2007). Elucidation of a universal size-control mechanism in Drosophila and mammals. Cell *130*, 1120–1133.

Dotti, C.G., Sullivan, C.A., and Banker, G.A. (1988). The establishment of polarity by hippocampal neurons in culture. J. Neurosci. *8*, 1454–1468.

Duning, K., Schurek, E.M., Schlüter, M., Bayer, M., Reinhardt, H.C., Schwab, A., Schaefer, L., Benzing, T., Schermer, B., Saleem, M.A., et al. (2008). KIBRA modulates directional migration of podocytes. J. Am. Soc. Nephrol. *19*, 1891–1903.

Duning, K., Wennmann, D.O., Bokemeyer, A., Reissner, C., Wersching, H., Thomas, C., Buschert, J., Guske, K., Franzke, V., Flöel, A., et al. (2013). Common exonic missense variants in the C2 domain of the human KIBRA protein modify lipid binding and cognitive performance. Transl. Psychiatry *3*, e272.

Elias, G.M., Funke, L., Stein, V., Grant, S.G., Bredt, D.S., and Nicoll, R.A. (2006). Synapse-specific and developmentally regulated targeting of AMPA receptors by a family of MAGUK scaffolding proteins. Neuron *52*, 307–320.

Feyder, M., Karlsson, R.M., Mathur, P., Lyman, M., Bock, R., Momenan, R., Munasinghe, J., Scattoni, M.L., Ihne, J., Camp, M., et al. (2010). Association of mouse Dlg4 (PSD-95) gene deletion and human DLG4 gene variation with phenotypes relevant to autism spectrum disorders and Williams' syndrome. Am. J. Psychiatry *167*, 1508–1517.

Frech, M.J., Rabenstein, M., Bovensiepen, K., Rost, S., and Rolfs, A. (2015). Cyclodextrin alters GABAergic input to CA1 pyramidal cells in wild-type but not in NPC1-deficient mice. Biores. Open Access *4*, 358–362.

Fukuda, T., Nagashima, S., Inatome, R., and Yanagi, S. (2019). CAMDI interacts with the human memory-associated protein KIBRA and regulates AMPAR cell surface expression and cognition. PLoS One *14*, e0224967.

Futai, K., Kim, M.J., Hashikawa, T., Scheiffele, P., Sheng, M., and Hayashi, Y. (2007). Retrograde modulation of presynaptic release probability through signaling mediated by PSD-95-neuroligin. Nat. Neurosci. *10*, 186–195.

Gabriel, L.R., Wu, S., and Melikian, H.E. (2014). Brain slice biotinylation: an ex vivo approach to measure region-specific plasma membrane protein trafficking in adult neurons. J. Vis. Exp.

Gan, L., Cookson, M.R., Petrucelli, L., and La Spada, A.R. (2018). Converging pathways in neurodegeneration, from genetics to mechanisms. Nat. Neurosci. *21*, 1300–1309.

Genevet, A., Wehr, M.C., Brain, R., Thompson, B.J., and Tapon, N. (2010). Kibra is a regulator of the Salvador/Warts/Hippo signaling network. Dev. Cell *18*, 300–308.

Goslin, K., Asmussen, H., and Banker, G. (1998). In Culturing Nerve Cells: Rat Hippocampal Neurons in Low-Density Culture, G. Banker and K. Goslin, eds. (MIT Press), pp. 339–370.

Granger, A.J., Shi, Y., Lu, W., Cerpas, M., and Nicoll, R.A. (2013). LTP requires a reserve pool of glutamate receptors independent of subunit type. Nature *493*, 495–500.

Groc, L., and Choquet, D. (2020). Linking glutamate receptor movements and synapse function. Science *368*, eaay4631.

Heitz, F.D., Farinelli, M., Mohanna, S., Kahn, M., Duning, K., Frey, M.C., Pavenstädt, H., and Mansuy, I.M. (2016). The memory gene KIBRA is a bidirectional regulator of synaptic and structural plasticity in the adult brain. Neurobiol. Learn. Mem. *135*, 100–114.

Husain, M., and Mehta, M.A. (2011). Cognitive enhancement by drugs in health and disease. Trends Cogn. Sci. *15*, 28–36.

Ji, Z., Li, H., Yang, Z., Huang, X., Ke, X., Ma, S., Lin, Z., Lu, Y., and Zhang, M. (2019). Kibra modulates learning and memory via binding to Dendrin. Cell Rep. *26*, 2064–2077.e7. e2067.

Johannsen, S., Duning, K., Pavenstädt, H., Kremerskothen, J., and Boeckers, T.M. (2008). Temporal-spatial expression and novel biochemical properties of the memory-related protein KIBRA. Neuroscience *155*, 1165–1173.

Kato, A.S., Burris, K.D., Gardinier, K.M., Gernert, D.L., Porter, W.J., Reel, J., Ding, C., Tu, Y., Schober, D.A., Lee, M.R., et al. (2016). Forebrain-selective AMPA-receptor antagonism guided by TARP gamma-8 as an antiepileptic mechanism. Nat. Med. *22*, 1496–1501.

Koopmans, F., van Nierop, P., Andres-Alonso, M., Byrnes, A., Cijsouw, T., Coba, M.P., Cornelisse, L.N., Farrell, R.J., Goldschmidt, H.L., Howrigan, D.P., et al. (2019). SynGO: an evidence-based, expert-curated knowledge base for the synapse. Neuron *103*, 217–234.e4.

Kopec, C.D., Li, B., Wei, W., Boehm, J., and Malinow, R. (2006). Glutamate receptor exocytosis and spine enlargement during chemically induced long-term potentiation. J. Neurosci. *26*, 2000–2009.

Kremerskothen, J., Plaas, C., Büther, K., Finger, I., Veltel, S., Matanis, T., Liedtke, T., and Barnekow, A. (2003). Characterization of KIBRA, a novel WW domain-containing protein. Biochem. Biophys. Res. Commun. *300*, 862–867.

Kremerskothen, J., Plaas, C., Kindler, S., Frotscher, M., and Barnekow, A. (2005). Synaptopodin, a molecule involved in the formation of the dendritic spine apparatus, is a dual actin/alpha-actinin binding protein. J. Neurochem. *92*, 597–606.

Lei, Q.Y., Zhang, H., Zhao, B., Zha, Z.Y., Bai, F., Pei, X.H., Zhao, S., Xiong, Y., and Guan, K.L. (2008). TAZ promotes cell proliferation and epithelial-mesenchymal transition and is inhibited by the hippo pathway. Mol. Cell Biol. *28*, 2426–2436.

Lin, Z., Yang, Z., Xie, R., Ji, Z., Guan, K., and Zhang, M. (2019). Decoding WW domain tandem-mediated target recognitions in tissue growth and cell polarity. Elife *8*, e49439.

Loh, K.H., Stawski, P.S., Draycott, A.S., Udeshi, N.D., Lehrman, E.K., Wilton, D.K., Svinkina, T., Deerinck, T.J., Ellisman, M.H., Stevens, B., et al. (2016). Proteomic analysis of unbounded cellular compartments: synaptic clefts. Cell *166*, 1295–1307.e21.

Lynch, G., Cox, C.D., and Gall, C.M. (2014). Pharmacological enhancement of memory or cognition in normal subjects. Front. Syst. Neurosci. *8*, 90.

Maccarrone, G., Bonfiglio, J.J., Silberstein, S., Turck, C.W., and Martins-de-Souza, D. (2017). Characterization of a protein interactome by Co-immunoprecipitation and shotgun mass spectrometry. Methods Mol. Biol. *1546*, 223–234.

MacGillavry, H.D., Song, Y., Raghavachari, S., and Blanpied, T.A. (2013). Nanoscale scaffolding domains within the postsynaptic density concentrate synaptic AMPA receptors. Neuron *78*, 615–622.

Makuch, L., Volk, L., Anggono, V., Johnson, R.C., Yu, Y., Duning, K., Kremerskothen, J., Xia, J., Takamiya, K., and Huganir, R.L. (2011). Regulation of AMPA receptor function by the human memory-associated gene KIBRA. Neuron *71*, 1022–1029.

Martín-Belmonte, A., Aguado, C., Alfaro-Ruíz, R., Itakura, M., Moreno-Martínez, A.E., de la Ossa, L., Molnár, E., Fukazawa, Y., and Luján, R. (2020). Age-dependent shift of AMPA receptors from synapses to intracellular compartments in alzheimer's disease: immunocytochemical analysis of the CA1 hippocampal region in APP/PS1 transgenic mouse model. Front. Aging Neurosci. *12*, 577996.

Masters, C.L., Bateman, R., Blennow, K., Rowe, C.C., Sperling, R.A., and Cummings, J.L. (2015). Alzheimer's disease. Nat. Rev. Dis. Primers *1*, 15056.

Matt, L., Kim, K., Hergarden, A.C., Patriarchi, T., Malik, Z.A., Park, D.K., Chowdhury, D., Buonarati, O.R., Henderson, P.B., Gökçek Saraç, Ç., et al. (2018). Alpha-actinin anchors PSD-95 at postsynaptic sites. Neuron *97*, 1094–1109.e9.

Millan, M.J., Agid, Y., Brüne, M., Bullmore, E.T., Carter, C.S., Clayton, N.S., Connor, R., Davis, S., Deakin, B., DeRubeis, R.J., et al. (2012). Cognitive dysfunction in psychiatric disorders: characteristics, causes and the quest for improved therapy. Nat. Rev. Drug Discov. *11*, 141–168.

Milnik, A., Heck, A., Vogler, C., Heinze, H.J., de Quervain, D.J., and Papassotiropoulos, A. (2012). Association of KIBRA with episodic and working memory: a meta-analysis. Am. J. Med. Genet. Part B, Neuropsychiatric genetics : the official publication of the International Society of Psychiatric Genetics *159B*, 958–969.

Mondin, M., Labrousse, V., Hosy, E., Heine, M., Tessier, B., Levet, F., Poujol, C., Blanchet, C., Choquet, D., and Thoumine, O. (2011). Neurexin-neuroligin adhesions capture surface-diffusing AMPA receptors through PSD-95 scaffolds. J. Neurosci. *31*, 13500–13515.

Moore, C.I., Browning, M.D., and Rose, G.M. (1993). Hippocampal plasticity induced by primed burst, but not long-term potentiation, stimulation is impaired in area CA1 of aged Fischer 344 rats. Hippocampus *3*, 57–66.

Nicoll, R.A., Tomita, S., and Bredt, D.S. (2006). Auxiliary subunits assist AMPA-type glutamate receptors. Science *311*, 1253–1256.

Papassotiropoulos, A., Stephan, D.A., Huentelman, M.J., Hoerndli, F.J., Craig, D.W., Pearson, J.V., Huynh, K.D., Brunner, F., Corneveaux, J., Osborne, D., et al. (2006). Common Kibra alleles are associated with human memory performance. Science *314*, 475–478.

Park, J., Chávez, A.E., Mineur, Y.S., Morimoto-Tomita, M., Lutzu, S., Kim, K.S., Picciotto, M.R., Castillo, P.E., and Tomita, S. (2016). CaMKII phosphorylation of TARPgamma-8 is a mediator of LTP and learning and memory. Neuron *92*, 75–83.

Penn, A.C., Zhang, C.L., Georges, F., Royer, L., Breillat, C., Hosy, E., Petersen, J.D., Humeau, Y., and Choquet, D. (2017). Hippocampal LTP and contextual learning require surface diffusion of AMPA receptors. Nature *549*, 384–388.

Perez-Riverol, Y., Bai, J., Bandla, C., García-Seisdedos, D., Hewapathirana, S., Kamatchinathan, S., Kundu, D.J., Prakash, A., Frericks-Zipper, A., Eisenacher, M., et al. (2022). The PRIDE database resources in 2022: a Hub for mass spectrometry-based proteomics evidences. Nucleic Acids Res. *50*, D543–D552.

Rappsilber, J., Mann, M., and Ishihama, Y. (2007). Protocol for micro-purification, enrichment, pre-fractionation and storage of peptides for proteomics using StageTips. Nat Protoc *2*, 1896–1906.

Rouach, N., Byrd, K., Petralia, R.S., Elias, G.M., Adesnik, H., Tomita, S., Karimzadegan, S., Kealey, C., Bredt, D.S., and Nicoll, R.A. (2005). TARP gamma-8 controls hippocampal AMPA receptor number, distribution and synaptic plasticity. Nat. Neurosci. *8*, 1525–1533.

Schnell, E., Sizemore, M., Karimzadegan, S., Chen, L., Bredt, D.S., and Nicoll, R.A. (2002). Direct interactions between PSD-95 and stargazin control synaptic AMPA receptor number. Proc. Natl. Acad. Sci. USA *99*, 13902–13907.

Schwenk, J., Harmel, N., Brechet, A., Zolles, G., Berkefeld, H., Müller, C.S., Bildl, W., Baehrens, D., Hüber, B., Kulik, A., et al. (2012). High-resolution proteomics unravel architecture and molecular diversity of native AMPA receptor complexes. Neuron *74*, 621–633.

Setou, M., Seog, D.H., Tanaka, Y., Kanai, Y., Takei, Y., Kawagishi, M., and Hirokawa, N. (2002). Glutamate-receptor-interacting protein GRIP1 directly steers kinesin to dendrites. Nature *417*, 83–87.

Shin, H., Wyszynski, M., Huh, K.H., Valtschanoff, J.G., Lee, J.R., Ko, J., Streuli, M., Weinberg, R.J., Sheng, M., and Kim, E. (2003). Association of the kinesin motor KIF1A with the multimodular protein liprin-alpha. J. Biol. Chem. *278*, 11393–11401.

Temkin, P., Morishita, W., Goswami, D., Arendt, K., Chen, L., and Malenka, R. (2017). The retromer supports AMPA receptor trafficking during LTP. Neuron *94*, 74–82.e5.

Thomas, P.D., Campbell, M.J., Kejariwal, A., Mi, H., Karlak, B., Daverman, R., Diemer, K., Muruganujan, A., and Narechania, A. (2003). PANTHER: a library of protein families and subfamilies indexed by function. Genome Res. *13*, 2129–2141.

Tracy, T.E., Sohn, P.D., Minami, S.S., Wang, C., Min, S.W., Li, Y., Zhou, Y., Le, D., Lo, I., Ponnusamy, R., et al. (2016). Acetylated tau Obstructs KIBRA-mediated signaling in synaptic plasticity and promotes Tauopathy-related memory loss. Neuron *90*, 245–260.

Tyanova, S., Temu, T., Sinitcyn, P., Carlson, A., Hein, M.Y., Geiger, T., Mann, M., and Cox, J. (2016). The Perseus computational platform for comprehensive analysis of (prote)omics data. Nat. Methods *13*, 731–740.

Vogt-Eisele, A., Krüger, C., Duning, K., Weber, D., Spoelgen, R., Pitzer, C., Plaas, C., Eisenhardt, G., Meyer, A., Vogt, G., et al. (2014). KIBRA (KIdney/BRAin protein) regulates learning and memory and stabilizes Protein kinase Mzeta. J. Neurochem. *128*, 686–700.

Wang, W., Li, X., Huang, J., Feng, L., Dolinta, K.G., and Chen, J. (2014). Defining the protein-protein interaction network of the human hippo pathway. Mol. Cell. Proteomics *13*, 119–131.

Weekes, M.P., Antrobus, R., Lill, J.R., Duncan, L.M., Hör, S., and Lehner, P.J. (2010). Comparative analysis of techniques to purify plasma membrane proteins. J. Biomol. Tech. *21*, 108–115.

Xia, J., Zhang, X., Staudinger, J., and Huganir, R.L. (1999). Clustering of AMPA receptors by the synaptic PDZ domain-containing protein PICK1. Neuron *22*, 179–187.

Xiao, L., Chen, Y., Ji, M., and Dong, J. (2011). KIBRA regulates Hippo signaling activity via interactions with large tumor suppressor kinases. J. Biol. Chem. *286*, 7788–7796.

Yang, Y.J., Chen, H.B., Wei, B., Wang, W., Zhou, P.L., Zhan, J.Q., Hu, M.R., Yan, K., Hu, B., and Yu, B. (2015). Cognitive decline is associated with reduced surface GluR1 expression in the hippocampus of aged rats. Neurosci. Lett. *591*, 176–181.

Yu, F.X., Zhao, B., and Guan, K.L. (2015). Hippo pathway in organ size control, tissue homeostasis, and cancer. Cell *163*, 811–828.

STAR★METHODS

KEY RESOURCES TABLE

REAGENT or RESOURCE	SOURCE	IDENTIFIER
Antibodies		
anti-b-actin	Cell Signaling Technologies	Cat#8457; RRID:AB_10950489
anti-ANK3	Thermo Fisher Scientific	Cat#33–8800; RRID:AB_2533145
anti-AP2M1	Abcam	Cat#ab106542; RRID:AB_10863380
anti-MPP2	Abcam	Cat#ab231634; RRID: N/A
anti-BAIAP2	Sigma	Cat#HPA023310; RRID:AB_1845264
anti-SEPT7	Abcam	Cat#ab175229; RRID: N/A
anti-CACNB4	Abcam	Cat#ab85788; RRID:AB_1860050
anti-ACTN4	Thermo Fisher Scientific	Cat#42–1400; RRID:AB_2533514
anti-ARPC2	Abcam	Cat#ab133315; RRID: N/A
anti-HOMER1	Abcam	Cat#ab88827; RRID:AB_2041667
anti-EFNB3	Abcam	Cat#ab101699; RRID:AB_10860789
anti-RAC1	Thermo Fisher Scientific	Cat#PA1-091; RRID:AB_2539856
anti-NRXN1	Sigma	Cat#SAB4503629; RRID:AB_10747310
anti-ACTN1	Abcam	Cat#ab18061; RRID:AB_444218
anti-DLGAP2	Abcam	Cat#ab106520; RRID:AB_10858567
anti-PRKCZ	Cell Signaling Technologies	Cat#9368; RRID:AB_10693777
anti-LATS1	Cell Signaling Technologies	Cat#3477; RRID:AB_2133513
anti-LATS2	Cell Signaling Technologies	Cat#5888; RRID:AB_10835233
anti-KIBRA	Cell Signaling Technologies	Cat#8774; RRID:AB_10949111
anti-CACNG8/Tarpγ-8	Abcam	Cat#ab116142; RRID:AB_10900936
anti-HA	Cell Signaling Technologies	Cat#3724; RRID:AB_1549585
anti-FLAG	Sigma	Cat#F3165; RRID:AB_259529
anti-PICK1	Cell Signaling Technologies	Cat#85325; RRID:AB_2800051
anti-GRIP1	Thermo Fisher Scientific	Cat#PA5-67825; RRID:AB_2692230
anti-SAP97	Thermo Fisher Scientific	Cat#PA1-741; RRID:AB_2092020
anti-PSD95	Cell Signaling Technologies	Cat#2507; RRID:AB_561221
anti-CASK	Cell Signaling Technologies	Cat#2878; RRID:AB_2068716
anti-PACSIN	Millipore	Cat#AB10439; RRID:AB_1977407
anti-SHISA6	Novus Biologicals	Cat#NBP1-93747; RRID:AB_11024576
anti-DNM1	Sigma	Cat#SAB2100611; RRID:AB_10604671
anti-SYNPO	Thermo Fisher Scientific	Cat#PA5-21062; RRID:AB_11156393
anti-YWHAB, 14-3-3 beta	Thermo Fisher Scientific	Cat#PA1-37002; RRID:AB_2217649
anti-AKAP5	Thermo Fisher Scientific	Cat#PA5-36155; RRID:AB_2553398
anti-NCAM1	Cell Signaling Technologies	Cat#99746; RRID:AB_2868490
anti-MYO6	Thermo Fisher Scientific	Cat#PA5-68238; RRID:AB_2691957
anti-CAMKIIa	Thermo Fisher Scientific	Cat#MA1-048; RRID:AB_325403
anti-KIF5B	Cell Signaling Technologies	Cat#18148; RRID: N/A
anti-DNAI1	Sigma	Cat#HPA021843; RRID:AB_1847914
anti-GLUA1	Cell Signaling Technologies	Cat#13185; RRID:AB_2732897
anti-GLUA2	Cell Signaling Technologies	Cat#5306; RRID:AB_10622024
anti-GLUA3	Cell Signaling Technologies	Cat#4676; RRID:AB_10547136
anti-rabbit IgG, HRP-linked	Cell Signaling Technologies	Cat#7074; RRID:AB_2099233
anti-mouse IgG, HRP-linked	Cell Signaling Technologies	Cat#7076; RRID:AB_330924

(*Continued on next page*)

Continued

REAGENT or RESOURCE	SOURCE	IDENTIFIER
Bacterial and virus strains		
AAV-pSyn-EGFP-WPRE-V1972	this paper	N/A
AAV-pSyn-KIBRA-var3-P37A-2xHA_V2037	this paper	N/A
AAV_SynP_KIBRA_var3_2xHA	this paper	N/A
AAV1/2sh-scr_160719	this paper	N/A
AAV_shWwc1_3_Syn1p_EGFP	this paper	N/A
Chemicals, peptides, and recombinant proteins		
Sulfo-NHS-SS-biotin	Pierce	Cat#21331
streptavidin beads	Thermo Fisher Scientific	Cat#11206D
protein G dynabeads	Invitrogen	100-03D
Rolipram	Cayman Chemical	Cat#10011132
Forskolin	Cayman Chemical	Cat#11018
Picrotoxin	Cayman Chemical	Cat#20771
Deposited data		
mass spectrometry proteomics data deposited to the ProteomeXchange Consortium via the PRIDE	this paper	PXD037756
Experimental models: Organisms/strains		
Mice: C57BL/6N	Max Planck Institute of Psychiatry	RRID: N/A
Mice: 129SV/C57BL6/N$^{Wwc1-/-}$ and 129SV/C57BL6/N$^{Wwc1+/+}$	Max Planck Institute of Psychiatry, PI: J. Kremerskothen, H. Pavenstädt	Makuch et al. (2011); RRID: N/A
Mice: C57BL/6N	University Hospital Bonn	RRID: N/A
Recombinant DNA		
AAV-pSyn-EGFP-WPRE-V1972	this paper	PI: M. Wehr
AAV-pSyn-KIBRA-var3-P37A-2xHA_V2037	this paper	PI: M. Wehr
AAV_SynP_KIBRA_var3_2xHA	this paper	PI: M. Wehr
AAV1/2sh-scr_160719	this paper	PI: M. Wehr
AAV_shWwc1_3_Syn1p_EGFP	this paper	PI: M. Wehr
Software and algorithms		
GraphPad Prism, Version 8	GraphPad Software, Inc.	RRID:SCR_002798
SynGO, Synaptic Gene Ontologies	Koopmans et al. (2019)	RRID: N/A
Panther Classification System	Thomas et al. (2003)	RRID:SCR_004869
MaxQuant	Cox and Mann (2008)	RRID:SCR_014485
ANY-maze, Version 7	Stoelting	RRID:SCR_014289
Perseus	Tyanova et al. (2016)	RRID:SCR_015753
Automated literature search, source code in STAR Methods section	this paper	RRID: N/A

RESOURCE AVAILABILITY

Lead contact

Further information, resources, and reagents are available from the lead contact, Nils C. Gassen (nils.gassen@ukbonn.de), upon reasonable request.

Materials availability

This study did not generate new unique reagents.

Data and code availability

The published article includes all datasets generated or analyzed during this study. Membranome and interactome unprocessed data see Tables S1, S2, S3.

The mass spectrometry proteomics data have been deposited to the ProteomeXchange Consortium via the PRIDE (Perez-Riverol et al., 2022) partner repository with the dataset identifier PXD037756.
All data reported in this paper will be shared by the lead contact upon request.
All original code is available in this paper's STAR Methods section.
Any additional information required to reanalyze the data reported in this paper is available from the lead contact upon request.

EXPERIMENTAL MODEL AND SUBJECT DETAILS

Mouse strains

Experiments were performed with group-housed adult (7–12 weeks), male mice, which were maintained in IVC racks (Greenline Tecniplast; equipped with bedding and wooden enrichment tubes) under standard laboratory conditions (temperature: 22°C ± 3°C, humidity: 50% ± 10%), *ad libitum* access to food and water. Mice were housed under a 12 h:12 h light-dark cycle (lights on at 06:00 h) in the vivarium of the Max Planck Institute of Psychiatry or University Hospital Bonn and were tested during the light phase. Animals were allowed to acclimatize for at least 7 days before starting experiments. If not stated otherwise, mice were kept on the C57BL/6N background and derived from internal breeding stocks (Max Planck Institute of Psychiatry, University Hospital Bonn). *Wwc1*-KO mice (Makuch et al., 2011; Vogt-Eisele et al., 2014) were maintained on a 129SV/C57BL6/N hybrid background. Experiments were performed on homozygous males (KO = $Wwc1^{-/-}$) and their age-matched littermate controls (WT = $Wwc1^{+/+}$). All animal studies were in agreement with the government of Upper Bavarian (AZ: ROB-55.2-2532.Vet_02-18-55) and were conducted in accordance with the recommendations of the Federation for Laboratory Animal Science Associations and according to the European Community Council Directive 2010/63/EEC.

Primary cell cultures

Primary hippocampal neurons were prepared from C57BL/6N mouse embryos (E17.5–18.5, sex of the embryos was not determined) and maintained in Neurobasal-A medium with 2% B27 and 0.5 mM GlutaMAX-I (Gibco) at 37°C and 5% CO_2 (Dotti et al., 1988; Goslin et al., 1998).

METHOD DETAILS

Chemicals

Isoflurane (Isofluran CP®, cp-pharma) was used at a concentration of 1.0–2.5%. Rolipram (#10011132), Forskolin (#11018) and Picrotoxin (#20771) (all Cayman Chemical) were dissolved in DSMO to generate stock solutions of 1 mM, 50 mM and 100 mM, respectively. Sulfo-NHS-SS-biotin (Pierce, #21331) was dissolved in DMSO to generate a 200 mg/mL stock solution.

Chemical long-term potentiation (cLTP)

7 weeks old mice were anesthetized with Isoflurane and decapitated. All following steps were done in ice-cold, sucrose-based saline saturated with carbogen gas (95% O_2/5% CO_2). This saline (adjusted to pH 7.3–7.4) consisted of (in mM): 87 mM NaCl, 2.5 mM KCl, 25 mM $NaHCO_3$, 1.25 mM NaH_2PO_4 x H_2O, 10 mM Glucose x H_2O, 75 mM Sucrose, 0.5 mM $CaCl_2$ x 2 H_2O, 7 mM $MgCl_2$ x 6 H_2O. Hemispheres were separated to obtain slices from each animal for the control and cLTP group. Subsequently, 400 μm-thick transversal slices were prepared as previously described (Bischofberger et al., 2006; Frech et al., 2015; α-angle of ~10° and a β-angle of 0°) using a vibratome (Leica VT1200S; amplitude = 1 mm; speed = 0.1 mm/s). Afterward, slices were stored at 34°C for at least 30 min in carbogenated ACSF. This saline (adjusted to pH 7.3–7.4) consisted of (in mM): 130 NaCl; 2.75 KCl; 1.43 $MgSO_4$; 2.5 $CaCl_2$; 1.1 NaH_2PO_4; 28,82 $NaHCO_3$; 5 HEPES and 11 D-glucose. For chemical induction of long-term potentiation (cLTP), sections were transferred to carbogenated ACSF containing 100 nM rolipram, 50 μM forskolin, and 100 μM picrotoxin and incubated for 15 min at room temperature (RT) (carbogenated ACSF with 0.21% DMSO for controls) (Kopec et al., 2006). After an additional 5 or 15 min incubation period at RT in normal ACSF, slices were transferred to a plastic Petri dish and the hippocampi were punched out. Tissue from two sections (one from each hemisphere) was pooled in a reaction tube, centrifuged, snap frozen with LN2 and stored at −80°C until further analysis (see co-immunoprecipitation). Immunoprecipitates of protein extracts were analyzed using capillary-based immunoassays (Jess, ProteinSimple). When quantifying co-immunoprecipitated proteins, their signals were normalized to input protein and to the precipitated interactor protein.

Morris water maze (MWM)

The test was performed in a circular white pool with a diameter of 150 cm and 41 cm high walls that was placed on a table so that the edge of the wall was elevated 110 cm above the floor. The pool was filled with fresh tap water to a height of 33 cm on the first day before the first trial. The water temperature was maintained at 21 ± 1°C. The pool was localized in the middle of a cubic-like room (W309 cm x L357 cm x H283 cm), which contained prominent customized landmarks at the walls (rectangular, triangular and circular posters with different black/white patterns, fixed 170 cm above the floor), but no windows or additional prominent cues. The computer for video tracking was placed in the SW corner and a sink located in the NE corner, both not visible to the animals from the pool.

The room was illuminated by indirect light with two spots facing to the wall, resulting in 11.5 lux at water surface level. The escape platform of clear acryl plexiglas (diameter: 10 cm) was placed in a fixed position in the NW quadrant 1 cm beneath the water surface and 35 cm away from the wall.

Mice were transported cage-wise from the holding to the adjacent training room, and placed in front of a heating lamp after completing all trials. As indicated in the respective paragraphs of the results section and/or figure legends, each animal had to perform 2 trials per day with differing starting positions over a period of 5 days and with an inter-trial interval of 3–7 min. The starting positions were assigned in random order out of 7 positions evenly distributed along the perimeter of the pool. For each trial, mice were gently placed on the water surface facing the wall, and the experimenter took a seat at a fixed position the room. If an animal climbed onto the platform, it remained there for further five seconds until the experimenter brought the animal back to its home cage with the help of a metal grid fixed to a stick. If an animal did not find the platform within 60 s, the experimenter guided the animal to the platform with the stick without touching the mouse and noted 61 s as escape latency.

Each trial was recorded and analyzed by ANY-maze (version: 7, Stoelting). We assessed the following main parameter: (i) the escape latency recorded during the first trial per day (as a measure of long-term memory formation which is not confounded by short-term memory processes at a given training day) and, (ii) escape latencies averaged over all training days. 24 h after the last training, animals performed a 60 s probe trial during which the platform was removed from the maze, and the animals were started from the quadrant opposite to the target quadrant. The video tracking software divided the pool into 4 virtual quadrants, and we assessed, (iii) the time the animals spent in each of the quadrants. We also used the software option to additionally present averaged heat maps of MWM exploration that illustrate the selectivity of searching.

Novel object recognition (NOR)

Experiments were performed in a Y-shaped setup (arm length: 30 cm, arm width: 10 cm, wall height: 15 cm; floor covered with bedding) under low-light conditions (<40 lux). After a 9 min habituation trial at d0, mice were place in the base arm, with two identical objects (screw nut 6 cm × 4 cm, or bottle 7 cm × 5 cm) in the end of the upper left and upper right arms, and allowed to explore the objects for 9 min at d1 (sampling). One or 14 days later, mice were placed back to the setup for 9 min whereby one familiar object (FO) was replaced by a novel object (NO). The setup equipped with new bedding after each trial. Object type, start position and position of FO and NO were completely randomized, and all sessions were videotaped. A trained observer who was unfamiliar to the experimental groups, object type and position scored offline the interaction time of the animals with each of the objects during the test phase. As measure of object recognition memory, we considered both the exploration time spent with each object as well as the ratio of investigation duration (RID), which was calculated as follows: (NO-FO)/(NO + FO).

Stereotactic virus injections

Stereotactic virus injections into the dorsal Hippocampus (AP -2.3, ML: 1.65; DV: 1.6 mm) took place under isoflurane anesthesia (1.0–2.5%, Isofluran CP, cp-pharma). Mice were placed onto a heating pad, eyes were covered by applying moisturizing ointment. Fur was shaved and the skin was cleaned and pretreated with lidocaine. Skin was opened, the periosteum was removed using a cotton swab and the cranial bones were cleaned with 3% H_2O_2. On basis of bregma and Lambda, a hole was drilled into the skull at the position of the coordinates. A hamilton syringe was used to inject 300 nL of AAV-pSyn-EGFP-WPRE-V1972, AAV-pSyn-KIBRA-var3-P37A-2xHA_V2037, AAV_SynP_KIBRA_var3_2xHA, AAV1/2sh-scr_160719 or AAV_shWwc1_3_Syn1p_EGFP at a rate of 100 nL min^{-1} bilaterally. Analgesia was applied pre- (Metamizol 200 mg kg^{-1} (Merck), s.c.; Metacam, 5 mg kg^{-1} (Boehringer-Ingelheim), s.c.) and postsurgically (Metacam, 5 mg kg^{-1}, as required; p.o.).

Membrane protein biotinylation

Mouse hippocampal slices were washed (3 x ice-cold ACSF) and biotinylated with 1 mg/mL^{-1} sulfo-NHS-SS-biotin in ACSF on ice for 45 min. After washing (3 x ice-cold ACSF) and 10 min incubation on ice slices were washed in slice quench buffer (3 x ice-cold, 125 mM NaCl, 2.5 mM KCl, 1.2 mM NaH_2PO_4, 1.2 mM $MgCl_2$, 2.4 mM $CaCl_2$, 26 mM $NaHCO_3$, and 11 mM glucose, 100 mM glycine) and incubated in slice quench buffer for two times 25 min on ice. Slices were washed again (3 x ice-cold.

150 ACSF) and lysed in ice-cold RIPA buffer (10 mM Tris, pH 7.4, 150 mM NaCl, 1.0 mM EDTA, 1% Triton X-100, 0.1% SDS, 1% Na deoxycholate) supplemented with protease inhibitors (PI; Merck Millipore) for 30 min at 4°C while rotating. The centrifugation-cleared (15 min, 4°C, 18,000 x g) supernatant was used for streptavidin precipitation using magnetic streptavidin beads (Thermo, #11206D). A fraction of lysate was stored for Western blotting. Beads were equilibrated in RIPA (3 x at room temperature) and added to the lysates. Binding was performed by rotating the tubes (Protein LoBind Tubes 1.5 mL, Eppendorf) overnight at 4°C. Beads were washed (3 x RIPA + PI) and pellet was either air dried and send to proteomics or eluted in 2 x SDS-PAGE reducing sample buffer (30 min at room temperature). Lysates and elutes were analyzed by Western blotting.

Biotinylation efficiency using dot blot

A volume of 1 μL protein extracts from biotinylated tissue slices (as described above) corresponding to a total of 2 μg of protein was applied dot-wise to a dry methanol-activated PVDF membrane (BioRad). The membrane was left to dry for 10 min and subsequently placed in Tris-buffered saline, supplemented with 0.05% Tween (TBS-T, Sigma-Aldrich) and 5% non-fat milk (Carl Roth) for 1 h at room temperature while gentle agitation.

For the detection of biotinylated proteins, the membrane was probed with Streptavidin-HRP (Protein Simple) at a dilution of 1:1,000 in TBS-T for 1 h at room temperature while gentle agitation. After three 5 min washes with TBS-T, Streptavidin-biotin conjugates were visualized using ECL detection reagent (BioRad). Determination of the dot intensities were performed with BioRad, ChemiDoc MP.

Immunoblot analysis

Protein extracts were obtained by lysing cells in Pierce IP lysis buffer (150 mM NaCl, 1% NP-40, 1 mM EDTA, 5% glycerol, 25 mM Tris-HCl (pH7.4), Thermo Fisher Scientific) freshly supplemented with protease inhibitor (Merck Millipore), benzonase (Merck Millipore), 5 mM DTT (Sigma-Aldrich), and 1% PhosSTOP phosphatase inhibitor (Roche). Proteins were separated by SDS-PAGE and electro-transferred onto PVDF membranes or were analyzed using semi-automated capillary-based immunoassays (Jess, ProteinSimple). Blots were placed in Tris-buffered saline, supplemented with 0.05% Tween (Sigma-Aldrich) and 5% non-fat milk for 1 h at room temperature and then incubated with primary antibody (diluted in TBS/0.05% Tween) overnight at 4°C while shaking. The following primary antibodies were used: beta-actin (1:5,000 Cell Signaling Technology, #8457), ANK3 (1:1,000 Thermo Fisher, #33–8800), AP2M1 (1:1,000 ABCAM, ab106542), MPP2 (1:1,000 ABCAM, ab231634), BAIAP2 (1:1,000 Sigma, HPA023310), SEPT7 (1:1,000 ABCAM, ab175229), CACNB4 (1:1,000 ABCAM, ab85788), ACTN4 (1:1,000 Thermo Fisher, #42–1400), ARPC2 (1:1,000 ABCAM, ab133315), HOMER1 (1:1,000 ABCAM, ab88827), EFNB3 (1:1,000 ABCAM, ab101699), RAC1 (1:1,000 Thermo Fisher, #PA1-091), NRXN1 (1:1,000 Sigma, SAB4503629), ACTN1 (1:1,000 ABCAM, ab18061), DLGAP2 (1:1,000 ABCAM, ab106520), PRKCZ (1:1,000 Cell Signaling Technology, #9368), LATS1 (1:1,000 Cell Signaling Technology, #3477), LATS2 (1:1,000 Cell Signaling Technology, #5888), KIBRA (1:1,000 Cell Signaling Technology, #8774), CACNG8/TARPγ-8 (1:1,000 ABCAM, ab116142), HA (1:8,000 Cell Signaling Technology, #3724), FLAG (1:1,000 Sigma, F3165), PICK1 (1:1,000 Cell Signaling Technology, #85325), GRIP1 (1:1,000 Thermo Fisher, #PA5-67825), SAP97 (1:1,000 Thermo Fisher, #PA1-741), PSD95 (1:1,000 Cell Signaling Technology, #2507), CASK (1:1,000 Cell Signaling Technology, #2878), PACSIN (1:1,000 Millipore, AB10439), SHISA6 (1:11,000 Novus Biologicals NBP1-93747), DNM1 (1:1,000 Sigma SAB2100611), SYNPO (1:1,000 Thermo Fisher, #PA5-21062), YWHAB (1:1,000 Thermo Fisher, #PA1-37002), AKAP5 (1:1,000 Thermo Fisher, #PA5-36155), NCAM1 (1:1,000 Cell Signaling Technology, #99746), MYO6 (1:1,000 Thermo Fisher, #PA5-68238), CAMKIIα (1:1,000 Thermo Fisher, #MA1-048), KIF5B (1:1,000 Cell Signaling Technology, #18148), DNAI1 (1:1,000 Sigma HPA021843), GLUA1 (1:1,000 Cell Signaling Technology, #13185), GLUA2 (1:1,000 Cell Signaling Technology, #5306), GLUA3 (1:1,000 Cell Signaling Technology, #4676), Secondary antibodies: anti-rabbit IgG, HRP-linked antibody (1:10,000, Cell Signaling Technology, #7074), anti-mouse IgG, HRP-linked antibody (1:10,000, Cell Signaling Technology, #7076).

Subsequently, blots were washed and probed with the respective horseradish peroxidase- (or fluorophore-conjugated) secondary antibody for 1 h at room temperature. The immuno-reactive bands were visualized using ECL detection reagent (BioRad). Determination of the band intensities were performed with BioRad, ChemiDoc MP.

In general, protein quantification was performed by normalization to the intensity of actin, which was determined on the same membrane. For quantification of phosphorylated proteins this signal was always referred to the signal intensity of the corresponding total protein.

Transfections

Primary hippocampal neurons were either transfected using AAVs or by nucleofection. For nucleofection cells (2×10^6) were resuspended in 100 μL of transfection buffer (50 mM HEPES (pH 7.3), 90 mM NaCl, 5 mM KCl, and 0.15 mM $CaCl_2$). Up to 2 μg of plasmid DNA was added to the cell suspension, and electroporation was carried out using the Amaxa 2B-Nucleofector system (Lonza). Cells were replated at a density of 10^5 cells/cm^2.

Co-immunoprecipitation (Co-IP)

Immunoprecipitations of HA-tagged proteins or endogenous TARPγ-8 were performed using protein extracts (n = 4 per group) from hippocampus of control-AAV, HA-WWC1, HA-WWC1**-infected or shWwc1-infected mice or from mouse hippocampal primary cells transformed with the same AAVs. Briefly, 500 μg of lysate was incubated overnight with 2 μg of the appropriate IP-antibody (HA (Cell Signaling Technologies, #3724), (TARPγ-8 (ABCAM, ab116142) or IgG as control; FLAG (Sigma, F3165); and LATS2 (Cell Signaling Technologies, #5888) at 4°C. 20 μL of protein G dynabeads (Invitrogen, 100-03D) was blocked with BSA and subsequently added to the lysate-antibody mix and allowed to incubate at 4°C for 3 h in order to mediate binding between the dynabeads and the antibody-antigen complex of interest. The beads were washed three times with ice-cold PBS and either sent for proteomics or eluted as follows for Western blotting. The protein-antibody complexes were eluted with 60 μL Laemmli loading buffer. Thereafter, the eluate was boiled for 5 min at 95°C. Then 2–5 μL of each immunoprecipitate reaction product was separated by SDS-PAGE and electro-transferred onto nitrocellulose membranes.

Label-free quantitative proteomic analysis of membrane proteins and WWC1 interaction partners

For reduction and alkylation of the proteins, PBS washed magnetic beads were incubated with SDC buffer (1% Sodiumdeoxycholate, 40 nM 2-Cloroacetamide (Sigma-Aldrich), 10 mM tris(2-carboxyethyl)phosphine (TCEP, PierceTM, Thermo Fisher Scientific) in 100 mM Tris, pH 8.0) for 20 min at 37°C. Before digestion the samples were diluted 1:2 with MS grade water (VWR). Samples were digested overnight at 37°C with 1 μg trypsin (Promega).

After digestion, magnetic beads were separated from the supernatant with the help of a magnetic rack. The supernatants were collected in a new 1.5 mL reaction tube (Eppendorf) and acidified with Trifluoroacetic acid (Merck) to a final concentration of 1% and pH value of <2, followed by purification via SCX StageTips (Rappsilber et al., 2007), washed with 1% TFA in Isopropanol, followed by a second wash with 0.2% TFA, eluted as one fraction with 80% Acetonitrile and 5% Ammonia (Merck). Samples were vacuum dried and re-suspended in 6 μL of Buffer A (0.1% formic acid (Roth) in MS grade water (VWR).

Half of the purified samples were loaded onto a 15 cm column (inner diameter: 75 microns; packed in-house with ReproSil-Pur C18-AQ 1.9-micron beads, Dr. Maisch GmbH) via the autosampler of the Thermo Easy-nLC 1000 (Thermo Fisher Scientific) at 50°C. Using the nanoelectrospray interface, eluting peptides were directly sprayed into a Q Exactive HF mass spectrometer (Thermo Fisher Scientific).

Peptides were loaded in buffer A (0.1% (v/v) formic acid) at 250 nL min^{-1} and percentage of buffer B (80% acetonitrile, 0.1% formic acid) was ramped to 30% over 60 min followed by a ramp to 60% over 15 min then 95% over the next 5 min and maintained at 95% for another 10 min.

The mass spectrometer was operated in a data-dependent mode with survey scans from 300 to 1650 m/z (resolution of 60,000 at m/z = 200), and up to 15 of the top precursors were selected and fragmented using higher energy collisional dissociation (HCD with a normalized collision energy of value of 28). The MS2 spectra were recorded at a resolution of 15,000 (at m/z = 200). AGC target for MS and MS2 scans were set to 3E6 and 1E5 respectively within a maximum injection time of 100 and 25 ms for MS and MS2 scans respectively.

Raw data were processed using the MaxQuant (Cox and Mann, 2008) computational platform. The peak list was searched against Mouse Uniprot databases, with an initial precursor mass deviation up to 4.5 ppm for main search and an allowed fragment mass deviation of 20 ppm. MaxQuant by default enables individual peptide mass tolerance and was used in the search. Cysteine carbamidomethylation was set as the static modification, and methionine oxidation and N-terminal acetylation as variable modifications. The match between the run feature was enabled, and proteins were quantified across samples using the label-free quantification algorithm in MaxQuant as label-free quantification (LFQ) intensities. Notably, LFQ intensities do not reflect true copy numbers because they depend not only on the amounts of the peptides but also on their ionization efficiencies; thus, they only served to compare abundances of the same protein in different samples (for unprocessed data see Tables S1, S2, and S3).

Panther classification system

Proteins derived from the WWC1 interactome analysis were functionally classified using the PANTHER classification system (Thomas et al., 2003; v.15.0). A total of 1275 UniProtKB IDs out of 1408 were successfully mapped.

SynGO

SynGO annotated genes in the WWC1 interactome were derived from the geneset analysis using the SynGO knowledgebase (Koopmans et al., 2019) against a list of all brain expressed genes (default background set, specified as 'expressed in any GTEx v7 brain tissue'). For enrichment analysis, a 1-sided Fisher exact test with 'greater than' hypothesis was applied for each ontology term comparing the gene list against the background set. The GSEA 'gene cluster' FDR corrected p value (q-value) cutoff is >0.01.

Automated literature search

Protein lists resulting from the interactome analyses were subjected to an automated literature search performed with a custom python code, revealing as output the number of references found for each search. For the interactome list, the algorithm performed an automated PubMed search of the protein with "AMPA receptor" or "GluR1" or "GluR2" or "GluR3" or "GluR4" or "GluA1" or "GluA2" or "GluA3" or "GluA4" or "Gria1" or "Gria2" or "Gria3" or "Gria4". False positives resulting from protein name or abbreviation ambiguity were manually corrected.

```
import openpyxl as xl
import numpy as np
import xlsxwriter
from Bio import Entrez
def search(query):
Entrez.email = 'email' #enter email address
handle = Entrez.esearch(db = 'pubmed', sort = 'relevance',
retmax = '500', retmode = 'xml',
term = query)
results = Entrez.read(handle)
return results
def fetch_details(id_list):
ids = ','.join(id_list)
Entrez.email = 'email' #enter email address
handle = Entrez.efetch(db = 'pubmed', retmode = 'xml', id = ids)
```

```
results = Entrez.read(handle)
return results
wb = xl.load_workbook('file') #replace with excel file name
sheet = wb['workbook'] #replace with workbook name
howmanypapers = np.zeros(shape = [y,x]) #replace with workbook coordinates
allidlists = []
for row in range(y, sheet.max_row +1): #replace with workbook coordinates
try:
cell = sheet.cell(row, x) #replace with workbook coordinates
results = search(cell.value + '("AMPA receptor" OR GluR1 OR GluR2 OR GluR3 OR GluR4 OR GluA1 OR GluA2 OR GluA3 OR GluA4 OR Gria1 OR Gria2 OR Gria3 OR Gria4)')
id_list = results['IdList']
allidlists.append(id_list)
howmanypapers[row-2] = len(id_list)
finallist = ('row: ' + str(row) + ' for ' + cell.value + ' found ' + str(len(id_list)) + ' publications')
print(finallist)
except:
print('error reading cell ' + str(row))
```

QUANTIFICATION AND STATISTICAL ANALYSIS

Behavioral studies: To analyze the development of long-term memory formation in the MWM, we compared the development of escape latencies during the first trial per day over the course of training, using 2-way RM ANOVA, followed by post-hoc test as indicated in the corresponding figure legend. In addition, we compared the mean escape latencies over all training trials (unpaired t test), and the selectivity of spatial learning by considering the time the animals spent in each quadrant during the probe trial (2-way RM ANOVA), followed by post-hoc test as indicated in the corresponding figure legend. To reveal novel object recognition, we compared the investigation duration of the FO and NO separately per group (two-tailed paired t-tests), and the RIDs (two-tailed unpaired t-tests).

Membranome/Interactome: The Perseus software suite (v. 1.6.0.9; Tyanova et al., 2016) was used to filter out contaminants, reverse hits and protein groups, which were only identified by site. Only protein groups that were detected in at least 70% of the replicates of one condition were considered for the analysis.

The filtered data was log(2) transformed and missing values were imputed according to the normal distributed imputation algorithm implemented in the Perseus framework. Default values were used (width: 0.3; down shift: 1.8). To find the significantly regulated protein groups Students t Test, analysis of variance (ANOVA), and volcano plot analysis, were performed with a false discovery rate (FDR) correction for multiple testing.

All other data were analyzed by two-tailed paired/unpaired *t* test or by one-, or two-way ANOVA as appropriate using GraphPad Prism software (GraphPad Software, Inc., Version 8). Significant main or interaction effects were followed by Bonferroni or Tukey's post-hoc tests as appropriate. The criterion for significance was set at $p < 0.05$. For all data, results are shown as the mean ± s.e.m. All statistical details can be found in the figure legends and supplemental tables/figures.